EUROFUSION WPMST1-CP(16) 15057

M Willensdorfer et al.

Plasma response of magnetic perturbation at the edge: Comparisons between measurements and 3D MHD models

Preprint of Paper to be submitted for publication in
Proceedings of 26th IAEA Fusion Energy Conference

This work has been carried out within the framework of the EUROfusion Consortium and has received funding from the Euratom research and training programme 2014-2018 under grant agreement No 633053. The views and opinions expressed herein do not necessarily reflect those of the European Commission.

Plasma response of external magnetic perturbations at the edge: Comparisons between measurements and 3D MHD models

M. Willensdorfer[1], E. Strumberger[1], W. Suttrop[1], G. Birkenmeier[1,2], M. Cavedon[1,2], I. Classen[3], D. Brida[1,2], S.S. Denk[1,2], M. Dunne[1], S. Fietz[1], R. Fischer[1], L. Guimaris[11], V. Igochine[1], A. Kirk[4], Y. Q. Liu[4], A. Medvedeva[1,2,9,10], T. Odstrčil[1,2], D.A. Ryan[6,4], B. Vanovac[3], E. Viezzer[7], H. Zohm[1], I.C. Luhmann[8], the ASDEX Upgrade Team[1] and the EUROfusion MST1 Team[*]

[1]Max Planck Institute for Plasma Physics, 85748 Garching, Germany
[2]Physik-Department E28, Technische Universität München, 85748 Garching, Germany
[3]FOM-Institute DIFFER, Dutch Institute for Fundamental Energy Research
[4]CCFE, Culham Science Centre, Abingdon, Oxon, OX14 3DB, UK
[6]York Plasma Institute, University of York, Heslington, York,YO10 5DQ, UK
[7]Dept. of Atomic, Molecular and Nuclear Physics, University of Seville, Seville, Spain
[8]University of California at Davis, Davis, CA 95616, USA
[9]Institut Jean Lamour UMR 7198 CNRS, Universite de Lorraine, F-54000, Nancy, France
[10]CEA, IRFM, F-13108, St-Paul-Lez-Durance, France
[11]Instituto de Plasmas e Fuso Nuclear, Instituto Superior Tcnico, Universidade de Lisboa, 1049-001 Lisboa, Portugal
[*]See http://www.euro-fusionscipub.org/mst1

Corresponding Author: matthias.willensdorfer@ipp.mpg.de

Abstract:

Recent studies have shown that the mitigation and suppression of edge localized modes (ELMs) at low pedestal collisionality $\nu^\star$ using externally applied magnetic perturbations (MPs) are correlated with the excitation of ideal stable kink modes at the edge. These kink modes cause a three dimensional displacement of the plasma boundary, which is clamped to the applied MPs-field. The three dimensional boundary distortion induced by the ideal stable kink modes is measured using rigidly rotating MP-fields and toroidally localized high resolution diagnostics. Profile diagnostics, e.g. profile electron cyclotron emission (ECE), have been used to determine the amplitude of the flux surface displacements. Its dependence on the applied poloidal mode spectra have been studied by varying the differential phase between the MP-field from the upper and lower coil set. ECE-imaging (ECE-I) has been used to determine the dominant poloidal mode number of the displacement.

The measured displacement amplitudes at the outboard midplane are in good agreement with VMEC and clearly exceed the vacuum field calculations, when the ideal stable kink

modes are excited. Although the calculated magnetic structure of this edge kink peaks at poloidal mode numbers larger than the resonant components $|m| > |nq|$, the displacement derived from the ECE-I appears as mostly resonant. This is expected in ideal MHD in the proximity of rational surfaces. Both, VMEC and MARS-F calculations reproduce this experimental observation.

1 Introduction

Externally applied MPs can be used to mitigate and to suppress edge localized modes (ELMs) in high confinement mode (H-mode) [1]. At low collisionality, ELM mitigation and suppression are accompanied with a loss of confinement primarily due to the loss of density, the so called density 'pump-out'. Recent studies at AUG, DIII-D and MAST have shown that both, the best ELM mitigation as well as suppression are achieved by an externally applied MP-field, when its poloidal mode spectrum excites a mode at the edge, which is most amplified by the plasma [2–4]. According to magnetohydrodynamics (MHD) calculations [5], this mode is an ideal stable kink mode, which is driven by the H-mode edge pressure gradient and the associated bootstrap current. Because of the amplification by the plasma, the resulting MPs at the plasma boundary can be even larger than expected solely from the externally applied MP-field [6]. Moreover, this ideal stable kink mode causes a 3D distortion of the plasma boundary, which is static to the applied MP field. 3D MHD equilibrium codes, like JOREK [7,8], MARS-F [9], VMEC [10], etc. are capable to calculate this deformation for various plasma scenarios and coil configurations.

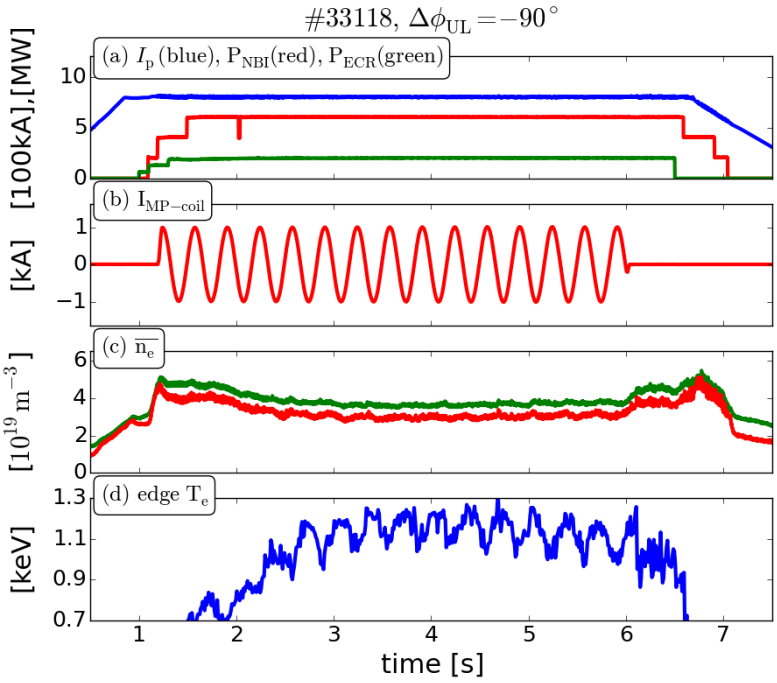

FIG. 1: Discharge overview: (a) plasma current, NBI and ECR heating, (b) power supply current of MP coil, (c) edge and core chord of line averaged density and (d) edge T_e from ECE.

The characterization and prediction of the non-axisymmetric boundary deformation is important since, for example, it can influence the coupling of ion cyclotron resonance heating (ICRH) antennas to the plasma or/and can cause unintended plasma movements

due to the plasma position control [11]. Furthermore, these MHD equilibrium codes predict that the X-point displacement maximizes when the poloidal mode spectrum is applied, which is best for ELM mitigation or even suppression. It is therefore assumed that the X-point displacement plays an important role for ELM mitigation.

In this paper, we characterize the plasma response via the 3D deformation of the plasma boundary. To vary the coupling of the externally applied MP field to the ideal stable kink mode, we changed its poloidal mode spectrum via the alignment between the field from the upper and lower coil set defined as differential phase angle ($\Delta\phi_{\mathrm{UL}}$). To measure the boundary displacements induced by the ideal stable kink mode, the MP-field is rigidly rotated resulting in a rigid rotation of the displacement induced by these kink modes. These measurements are then compared to 3D MHD equilibrium codes.

2 Setup

Experiments The present experiments were conducted using a toroidal field B_T of -2.5 T and a plasma current of 800 kA resulting in a safety factor of $q_{95} \sim -5.2$. The external heating power was around 7.5 and 1.5 MW from NBI and centrally deposited ECR heating, respectively (Fig. 1(a)). These discharges were immediately done after the boronization. This enabled us to achieve H-modes with high heating power at low density resulting in a low collisionality and high normalized beta (β_{N}) to observe a significant plasma response.

To measure the displacement, we use toroidally localized diagnostics and applied a rigidly rotating $n = 2$ MP-field. Figure 1 shows the time trace of the supplied current from one coil to indicate rigid rotation. To test the plasma response for different applied poloidal mode spectra, we varied the $\Delta\phi_{\mathrm{UL}}$ between the upper and lower coil set in-between discharges and even within the discharges. The resulting change of the applied poloidal mode spectra allows us to investigate its impact on the plasma response and the non-axisymmetric boundary displacement. In the presented discharge, $\Delta\phi_{\mathrm{UL}}$ was set to $-90°$ and we rotated the external MP-field with 3 Hz.

The amplitude of the displacement is primarily measured using the high resolution profile diagnostics of ASDEX Upgrade situated around the outer midplane. The set of used diagnostics consists of profile ECE [12,13], lithium beam (LIB) [14], edge charge exchange recombination spectroscopy (CXRS) [15], X-mode reflectometer (REF-X) and O-mode reflectometer (REF-O) [12]. To determine the dominant component of the poloidal mode spectrum of the displacement, we use the poloidal distribution of the ECE-imaging (ECE-I) diagnostic [16]. All these diagnostics have a high temporal resolution, which allows us to use pre-ELM time points only.

Modelling ASDEX Upgrade has a passive stabilization loop (PSL) to reduce the growth rate of vertical instabilities. It is a copper conductor situated very close to the MP-coils, which attenuates and delays the resulting MP-field at the plasma boundary depending on the applied frequency. We employ finite element calculations (FEM) calculations to obtain the attenuation and the delay [17]. According to these calculations, the MP-field

amplitude for a 2 Hz rotation is attenuated by 62.1% and 68.7% for the upper and lower coil set, respectively, whereas for 3 Hz the amplitude is 56.3% and 64.5%. The differences between the upper and lower coil set arises from different positions with respect to the PSL. The different PSL response for upper and lower coil has in a rigid rotation scan also a small effect on the differential phase $\Delta\phi_{\mathrm{UL}}$, which changes by not more than -4° for 3 Hz. To account for this attenuation, the response function from the FEM calculations are applied to the power supply current of the MP-coils. The result is an 'effective' coil current, which is used as input for the following modeling.

The simplest approximation to compare the measurements with is the vacuum field approximation. The vacuum field from the external MP-coils is simply superposed with the axisymmetric equilibrium field. The determination of a boundary displacement from vacuum field calculations is somewhat critical since a last closed flux surface (LCFS) is not necessarily preserved because of changes in the magnetic topology due to ergodization. However, one can define an 'effective' plasma boundary as the locus of the connection length exceeding a certain threshold value [18]. Since it is possible to calculate the connection length for the stable and unstable manifold, we determined the boundary from both separately. One should also keep in mind that these predictions ignore shielding of the applied MP-field and the amplification by ideal modes.

3D MHD equilibrium codes consider these effects and can be compared with experiments. One code, among others, which is the widely used is the VMEC equilibrium code. Its free boundary version can be used to include the non-axisymmetric MP-field via the boundary condition [10]. VMEC is an ideal MHD code [19] and assumes nested flux surfaces. Axisymmetric equilibria constrained by pre-ELM pressure profiles provide the initial input. The resulting 3D equilibrium solution is determined by minimizing the plasma energy (W_{MHD}). In VMEC, the geometry of the flux surfaces are given as Fourier series of the flux coordinates. The choice of a sufficient high grid resolution is essential. Otherwise, the calculated displacements could be underestimated. Hence, we choose 1001 flux surfaces, 17 toroidal mode numbers and 26 poloidal mode numbers for one period for all 3D VMEC calculations. A further increase of the resolution does not change the $n = 2$ displacement. But, there is also an upper limit for the grid resolution. The free boundary version of VMEC tends to oscillate at the boundary and corrupts the output when too many grid points are used.

3 Amplitude of the radial displacement

To investigate the impact of the applied poloidal mode spectra on the plasma response and the non-axisymmetric boundary displacement, we applied rigid rotating MP-fields with various $\Delta\phi_{\mathrm{UL}}$. The β_{N} varies during the $\Delta\phi_{\mathrm{UL}}$ scan because the plasma density reduction due to the MPs depends on $\Delta\phi_{\mathrm{UL}}$ [2]. This is accounted for by VMEC analysis for the lowest, the mean and the highest value of β_{N} encountered in the scan. The profile measurements are used to measure the change of the separatrix position during the rigid rotation. Here, we assume that global parameters do not vary during the rigid rotation, which is for example illustrated by the line integrated core density in figure 1. Furthermore, we

presume that plasma parameters like electron density (n_e), T_e, etc., are constant on the 3D flux surfaces during the rigid rotation. In the case of n_e profile measurements, the procedure is straight forward. The separatrix position can be easily tracked along the diagnostic lines of sight (LOS) using a separatrix density of 1.2 10^{19}m^{-3} during the rigid rotation. A similar procedure can be used for CXRS measurements. But instead of using the ion temperature (T_i) or the rotation profile, it is more advantageous to use the measured line intensity (I_{B5+}). T_i and rotation profiles are not reliable in the scrape off layer (SOL), because of a low measured line intensity. They usually exhibit large uncertainties and a large scatter. Because of the low beam attenuation at the edge, the line intensity is approximately proportional to the impurity density around the separatrix. Therefore, the line intensity profile increases monotonically from the SOL towards the pedestal top. This allows us to use the same procedure as for the n_e profile measurements. The separatrix value of the line intensity is determined either before the MP onset or during the rigid rotation. Because of the non-monotonic behavior of the radiation temperature (T_{rad}) profile from ECE at the edge (the 'shine-through' effect), ECE measurements require a different approach. In order to obtain the plasma displacement, first, we fit the T_{rad} data from the steep gradient region using a spline at the beginning of the rigid rotation [13]. Then, this spline is only varied by a radial shift until the least square (LSQ) is minimized. This is done for every time point throughout the analyzed time window.

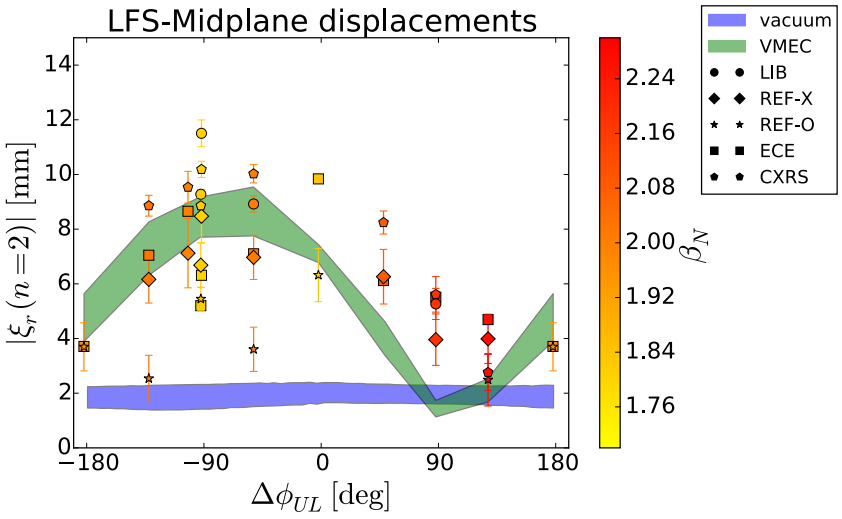

FIG. 2: Measured amplitudes of the radial displacement versus differential phase angle $\Delta\phi_{UL}$. The color scaling indicates β_N. Shaded areas span the range of VMEC (green) and vacuum field calculations (blue, stable and unstable manifold).

Since the amplitude of the ideal kink mode depends on the local pressure gradient and to be consistent with the 3D equilibrium calculations, we use only pre ELM data points. The amplitude of the displacement is determined by fitting the ELM-filtered time traces of the separatrix position using a sine function with given frequency. Finally, the amplitudes along the diagnostic LOS are mapped onto the normal of the axisymmetric flux surface, which allows a quantitive comparison between the measurements and the radial displacement from 3D equilibrium calculations. We applied this procedure to all diagnostics, which were operating during the various rigid rotation phases with the different values of $\Delta\phi_{UL}$s .

The comparison of the radial displacement amplitudes between the measurements and the VMEC as well as the vacuum field calculations using various $\Delta\phi_{\mathrm{UL}}$s are shown in figure 2. Good agreement can be found between the measurements and VMEC. When the ideal stable kink modes are expected to be excited, both surpass clearly the prediction from the vacuum field calculations, no matter which manifold is used. It is also seen from the green shaded area that the observed variation in β_{N} as well as in the edge pressure gradient have a moderate impact on the displacement amplitude.

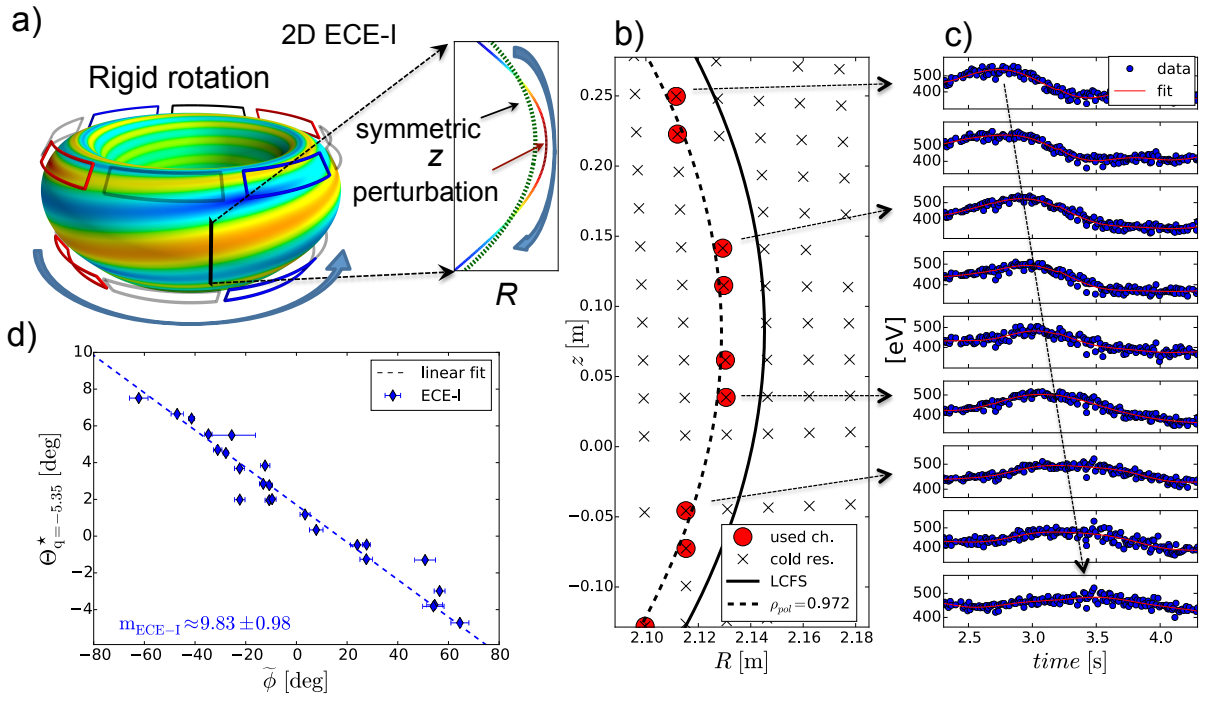

FIG. 3: (a) Measuring principle to determine the poloidal mode number from the alignment using the ECE-I. (b) (R,z) of ECE-I channels using the 'cold' resonance approximation, (c) Time traces of channels marked by red circles in (a). (d) SFL angles versus phase delays from ECE-I channels around the $q = -5.35$ surface. The poloidal mode number is obtained using $m = \frac{\Delta\phi}{\Delta\Theta^{\star}}$.

4 Poloidal mode structure

The poloidal resolution from imaging systems can be used to resolve the poloidal mode structure of the plasma displacement. Figure 3(a) shows the measuring principle. The MP-field and hence the ideal stable kink modes, which are static to the MP-field, are rotated in the positive toroidal direction. Since ASDEX Upgrade usually operates with negative toroidal field, the safety factor q is also negative. Therefore, the 3D structure should appear as a modulation, which propagates poloidally downwards. This is clearly seen in the time traces of selected ECE-I channels using only pre-ELM time points (fig-

ure 3(c)). The corresponding (R,z) positions from ECE-I where the measured frequency fulfills the electron cyclotron resonance condition (cold resonance position) are shown in figure 3(b).

Assuming a periodic distortion, the poloidal mode structure of the flux surface displacement can be characterized by using the Fourier decomposition of its normal component $\xi_r = |\xi_r|\ e^{i(n\phi+m\Theta^\star)}$, where $|\xi_r|$ is the amplitude, n the toroidal mode number, ϕ the toroidal angle, m the poloidal mode number and $\Theta^\star$ the SFL angle. One obtains the dominant poloidal mode number m using $m = \frac{\Delta\phi}{\Delta\Theta^\star}$, where $\Delta\phi$ and $\Delta\Theta^\star$ are the toroidal phase increment and the corresponding SFL angle difference between the various ECE-I channels. $\Delta\phi$ is determined by employing a simple sine fits to the ECE-I time traces (figure 3(c)). For an accurate determination of the calculated SFL angle, knowledge of the exact measurement positions are essential. Therefore, we extended the forward model of the electron cyclotron radiation transport from [12] with ray tracing [20] and applied it to the ECE-I system. Then, we determine the (R,z) measurement position of each channel using the maximum of the observed intensity distribution. These (R,z) positions are used to calculate $\Theta^\star$ on the $q = -5.35$ flux surface, which is in the mean of the used ECE-I channels (more details in Ref. [13]). Figure 3(d) shows the calculated $\Theta^\star$ versus $\Delta\phi$ of ECE-I measurements around the $q = -5.35$ surface. The dominant m is obtained from the slope of a linear fit and amounts to $m_{\mathrm{ECE-I}} \approx 9.8$, which is almost the same helicity as the axisymmetric equilibrium field (*resonant*).

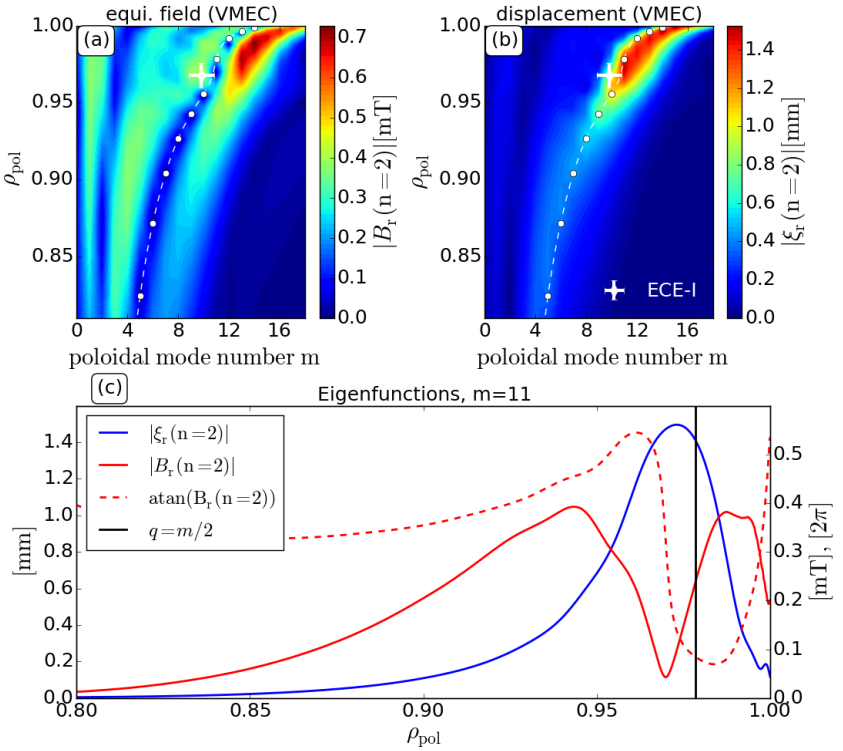

FIG. 4: Poloidal mode structure of the $n = 2$ amplitude from the radial perturbation of (a) the equilibrium field and (b) the flux surfaces. (c) The amplitudes of the radial Eigenfunctions using the $m = 11$ component and the corresponding phase angle from the MPs of the equilibrium field.

This ideal stable kink modes are usually referred to as *non-resonant* ideal stable kink modes, e.g. [6]. The reason for this is shown in figure 4(a), where the $n = -2$ poloidal mode spectra of the radial MP-amplitudes of the equilibrium field is plotted. The MPs peaks at poloidal mode numbers larger than the resonance condition $|m| > |nq|$ and is locally

minimized at the resonant surface. But, the radial displacement is almost aligned with the equilibrium field pitch, which is supported by ECE-I measurements. It is dominated by resonant components, which originate from the *non-resonant* ideal modes via poloidal mode coupling [21]. Hence, the radial displacement maximizes at the resonant surface where the MP of the equilibrium field minimizes. This is emphasized by figure 4(c), which shows the amplitudes of the corresponding radial $m = 11$ Eigenfunctions. Additionally, the phase angle from the perturbed equilibrium field is plotted and a phase jump of π is observed, where the MP amplitude minimizes and the displacement maximizes. This is expected from ideal MHD in the presence of rational surfaces. Interestingly, these typical characteristics for a sheet current on a rational surface are slightly displaced with respect to the associated rational surface determined by the iota profile from the VMEC output. This indicates a slight inconsistency in VMEC and one possible explanation could be an inappropriate handling of the localized sheet currents [22–24].

5 Summary

Rigid rotating MP-fields are used to measure the 3D surface displacement induced by ideal stable kink modes at the edge, which are excited by externally applied MP-fields. In general, good agreement between VMEC and the measurements is found. Using a sufficiently high resolution, VMEC correctly predicts the amplitude of the radial displacement on the outboard midplane. *Resonant* modes are found to dominate the displacement measured with ECE-I. This is expected from ideal MHD and reproduced in the VMEC solution. *Resonant* modes come in by toroidal and elongation mode coupling [21].

Acknowledgement This work has been carried out within the framework of the EUROfusion Consortium and has received funding from the Euratom research and training programme 2014-2018 under grant agreement No 633053. The views and opinions expressed herein do not necessarily reflect those of the European Commission.

References

[1] T. E. Evans et al. *Physical Review Letters*, 92:235003, 2004.
[2] C. Paz-Soldan et al. *Physical Review Letters*, 114:105001, 2015.
[3] A. Kirk et al. *Nuclear Fusion*, 55(4):043011, 2015.
[4] W. Suttrop et al. *submitted to Plasma Physics and Controlled Fusion*, 2016.
[5] Y. Q. Liu et al. *Nuclear Fusion*, 51(8):083002, 2011.
[6] R. A. Moyer et al. *Nuclear Fusion*, 52(12):123019, 2012.
[7] F. Orain et al. *Plasma Physics and Controlled Fusion*, 57(1):014020, 2015.
[8] F. Orain et al. *this conference*, TH/P126, 2016.
[9] Y. Q. Liu et al. *Physics of Plasma*, 7(9):3681, 2000.
[10] E. Strumberger et al. *Nuclear Fusion*, 54(6):064019, 2014.
[11] I. T. Chapman et al. *Plasma Physics and Controlled Fusion*, 56(7):075004, 2014.
[12] S. K. Rathgeber et al. *Plasma Physics and Controlled Fusion*, 55(2):025004, 2013.
[13] M. Willensdorfer et al. *Plasma Physics and Controlled Fusion*, 58(18):114004, 2016.
[14] M. Willensdorfer et al. *Plasma Physics and Controlled Fusion*, 56(2):025008, 2014.
[15] E. Viezzer et al. *Nuclear Fusion*, 54(1):012003, 2014.
[16] I. Classen et al. *Review of Scientific Instruments*, 85(11), 2014.
[17] W. Suttrop. Finite elements calculations from the saddle coils and the PSL. *private communication*, 2016.
[18] J. C. Fuchs et al. *41th EPS Conference on Plasma Phys.*, 2014.
[19] S. P. Hirshman et al. *Computer Physics Communications*, 43(1):143–155, 1986.
[20] S. S. Denk et al. *submitted to Plasma Physics and Controlled Fusion*, 2016.
[21] D. Ryan. et al. *Plasma Physics and Controlled Fusion*, 57(9):095008, 2015.
[22] A. Reimann et al. *Nuclear Fusion* 55:063026, 2014
[23] S. A. Lazerson et al. *Physics of Plasma*, 23(1):012507, 2016.
[24] J. Loizu. et al. *Physics of Plasma*, 23(5), 2016.